

‘Magnetic bandages’ for targeted delivery of therapeutic agents

M E Hayden¹ and U O Häfeli²

¹ Department of Physics, Simon Fraser University, 8888 University Drive, Burnaby, BC, V5A 1S6, Canada

² Faculty of Pharmaceutical Sciences, University of British Columbia, 2146 East Mall, Vancouver, BC, V6T 1Z3, Canada

E-mail: mhayden@sfu.ca and uhafeli@interchange.ubc.ca

Received 26 April 2006, in final form 23 June 2006

Published 8 September 2006

Online at stacks.iop.org/JPhysCM/18/S2877

Abstract

We investigate planar periodically magnetized structures for use in targeting or controlling the delivery of therapeutic agents attached to small magnetic particles, and derive simple analytic expressions for the relevant magnetostatic forces. We show that improved particle trapping or confinement characteristics are possible relative to those that can be obtained with more conventional (i.e. uniformly magnetized) structures. These improvements include forces that are larger at close range (for equivalent magnetization densities) and that are both unidirectional and uniform over arbitrarily large areas parallel to the magnet surface. Expressions for the magnetostatic forces exerted on point-like magnetic particles in the vicinity of long rods (with circular and ellipsoidal cross sections) uniformly magnetized perpendicular to their axes are summarized in an appendix.

(Some figures in this article are in colour only in the electronic version)

1. Introduction

The concept of a ‘magnetic bandage’ for targeting or controlling the delivery of therapeutic agents has considerable intuitive appeal [1]. A magnet, or an array of magnets—comprising the bandage—is placed near a lesion or tumour, and small highly permeable (i.e. magnetic) particles encapsulated with a protective coating and a drug or other agent are injected into the bloodstream. Magnetostatic forces acting on these particles cause them to become trapped against the walls of blood vessels in the region of interest (ROI). Next, the intended treatment is performed. This could involve anything ranging from the slow release of a chemotherapeutic drug or irradiation of tissues by beta emitters (contained within the particles) to localized hyperthermia induced by applying an alternating magnetic field. When the holding magnets are finally removed the particles either redistribute into the blood supply (and are eventually

cleared by the reticuloendothelial system) or remain within the ROI (as is the case when extravasation takes place). In both situations the residual toxicity is very low; magnetic particles (and in particular magnetite (Fe_3O_4) which is widely used for magnetic targeting applications) biodegrade (often after uptake by macrophages) and are recycled by the body. Within six weeks, the iron appears in the red blood cells [2]. Encouraging results from practical realizations of this drug targeting concept (involving both animal models [3, 4] and clinical trials with humans [5]) have helped to motivate a growing interest in developing, refining, and understanding [6–9] applications of magnetic nanoparticles to biomedicine [10].

A natural (but perhaps somewhat ill-defined) question that one can ask is ‘How should an external magnet or magnet array be designed and positioned so as to optimize its trapping efficiency?’ Clearly, some combination of magnetic fields and field gradients that give rise to large magnetostatic forces in the ROI is required. At the same time, the magnetic properties and size of the injected particles should be matched to the imposed fields and hydrodynamic forces so that the particles tend to concentrate in the desired location. A third consideration pertains to the manner in which the region of interest is perfused; this dictates both the injection site and to some extent the direction in which the imposed magnetostatic forces should act. One can certainly imagine a general scenario in which a suspension of particles with a range of properties would be injected so as to achieve a uniform or otherwise ‘tailored’ distribution (and hence activity) of the therapeutic agent in the presence of the magnetic bandage.

Here we investigate one aspect of the magnetic drug targeting problem: the design of magnetized structures for exerting large and—within physical constraints imposed by Maxwell’s equations—spatially uniform magnetostatic forces. In particular, we examine a class of planar structures characterized by the fact that magnetic flux can be made to emanate from only one of the two faces through an appropriate modulation of the magnetization vector [11, 12]. Many characteristics of these ‘one-sided flux’ structures are known in the context of devices as diverse as rubberized ‘refrigerator’ magnets, magnetic recording tape, undulators for the production of synchrotron radiation, and passive magnetic levitation systems [13–15], but to the best of our knowledge they have not been considered previously for magnetic trapping applications. Our analysis indicates that one-sided flux structures offer significant advantages over more conventional magnet designs in which the magnetization within the structure tends to be uniform.

Our treatment of this problem is by no means exhaustive. We ignore material properties and focus solely on geometric considerations. Moreover, no attempt is made to optimize magnet design for compatibility with various parts of the human body or to deal with finite size effects. Instead, we restrict our discussion to planar structures that are infinite in extent so as to be able to emphasize conceptual aspects of the design problem.

2. General considerations

A point-like particle with magnetic moment \mathbf{m} in a non-uniform but static magnetic induction \mathbf{B} is subject to a force $\mathbf{F} = \nabla(\mathbf{m} \cdot \mathbf{B})$. It also experiences a torque $\boldsymbol{\tau} = \mathbf{m} \times \mathbf{B}$ which, when combined with the dissipative influence of hydrodynamic forces, tends to bring \mathbf{m} into alignment with \mathbf{B} . If the magnetic susceptibility of the medium in which the particle is immersed is both small (as in the case for blood and biological tissues) and uniform³, the force \mathbf{F} can be written $\mathbf{F} = \mu_0 \nabla(\mathbf{m} \cdot \mathbf{H})$ or

$$\mathbf{F} = -\mu_0 \nabla(\mathbf{m} \cdot \nabla \phi_m), \quad (1)$$

³ Caution is required in the vicinity of interfaces between media. Differences in magnetic susceptibility can lead to situations in which this approximation is not valid.

where μ_0 is the permeability of free space, $\mathbf{H} = -\nabla\phi_m$ is the magnetic field associated with \mathbf{B} , and ϕ_m is the corresponding magnetic scalar potential.

To proceed further one needs to consider the magnetic response of the particle to changes in applied field. For the sake of clarity we simply distinguish between two limiting cases: that in which $|\mathbf{m}|$ increases in direct proportion to $|\mathbf{H}|$ and that in which $|\mathbf{m}|$ is independent of $|\mathbf{H}|$. We refer to these idealizations as unsaturated and saturated material responses, respectively, and note that intermediate situations are readily described through simple extensions of the arguments presented below. In the unsaturated case, which corresponds to the particle having a linear induced magnetic dipole moment (and is thus relevant to soft ferromagnetic and superparamagnetic materials in weak magnetic fields), \mathbf{m} can be written in the form

$$\mathbf{m} = \beta\mathbf{H}, \quad (2)$$

where β is a constant⁴. This leads to

$$\mathbf{F}_{\text{un}} = \mu_0\beta\nabla|\nabla\phi_m|^2. \quad (3)$$

In the saturated case, which corresponds to the particle having an intrinsic magnetic dipole moment m_s (and is thus relevant to single domain or permanently magnetized particles),

$$\mathbf{m} = m_s\mathbf{H}/H \quad (4)$$

and thus

$$\mathbf{F}_{\text{sat}} = \mu_0m_s\nabla|\nabla\phi_m|. \quad (5)$$

From a purely geometric perspective, the issue of trapping efficiency amounts to choosing the distribution of magnetic sources (magnetized materials and/or current distributions) that give rise to ϕ_m (or \mathbf{H}) in order to maximize (or otherwise optimize) the force exerted on point-like magnetic particles introduced into the bloodstream. Clearly ϕ_m and hence \mathbf{F} vary over a length scale determined by characteristic dimensions of its source, limiting the extent to which fields penetrate the body. This rule of thumb has previously motivated the selection and placement of uniformly magnetized blocks of material (typically rare-earth permanent magnets) with dimensions of order several centimetres so as to produce large fields in the vicinity of tumours during clinical trials [5]. Our presentation here is motivated by the simple observation that larger and (potentially more uniform) magnetostatic forces (cf equations (3) and (5)) can be generated through the judicious use of *non*-uniform magnetization distributions as sources of ϕ_m (or \mathbf{H}).

Two points are worth noting before proceeding. The first is related to the fact that one would like to exert large magnetostatic forces on point-like magnetic particles located within a well-defined ROI that is in general situated some distance from the surface of the body. This is not possible without also exerting large magnetostatic forces on particles located between the ROI and the external field source, a direct consequence of Earnshaw's Theorem [16]. That is, the nature of ϕ_m (the fact that it satisfies Laplace's equation in free space) is such that $\nabla\cdot\mathbf{F} = 0$ and thus local maxima in $|\mathbf{F}|$ can only exist adjacent to the source⁵. This implies that a careful choice of injection site and knowledge of the manner in which the ROI is perfused is necessary if magnetic particles are to be kept from entering and being trapped within the vasculature between the ROI and the source.

The second point is related to the distribution of magnetization that gives rise to ϕ_m (or \mathbf{H}), and the manner in which that distribution influences the field and its gradient at large distances.

⁴ In general β depends on geometry as well as the magnetic susceptibility of the particle and its surroundings. For example, $\beta = 3\chi V/2$ for a sphere of volume V and susceptibility $\chi \gg 1$ situated in free space and exposed to a uniform magnetic field. The arguments presented in this paper do not depend on such details.

⁵ This argument does not apply to particles with a diamagnetic response. See [7] for an illustration of this principle applied to two-dimensional magnetic fields.

The magnetic scalar potential for an arbitrary localized distribution of magnetization $\mathbf{M}(\mathbf{r})$ may be expressed as [17]

$$\phi_m(\mathbf{r}) = -\nabla \cdot \int_V \frac{\mathbf{M}(\mathbf{r}')}{|\mathbf{r} - \mathbf{r}'|} dV'. \quad (6)$$

Far away from the volume V in which \mathbf{M} is finite,

$$\phi_m(\mathbf{r}) \approx -\nabla \left(\frac{1}{r} \right) \cdot \int_V \mathbf{M}(\mathbf{r}') dV' = \frac{\mathbf{m}^* \cdot \mathbf{r}}{r^3}. \quad (7)$$

That is, ϕ_m asymptotically approaches the scalar potential of a magnetic dipole $\mathbf{m}^* = \int \mathbf{M}(\mathbf{r}') dV'$. An important distinction can be made between situations in which $m^* = 0$ and $m^* \neq 0$. If the distribution of \mathbf{M} is finite in two dimensions and uniform in the third, then at large enough distances ϕ_m (and hence \mathbf{H} , \mathbf{F}_{un} , and \mathbf{F}_{sat}) can always be expressed in terms of the magnetic scalar potential for an infinitely long (and appropriately magnetized) cylinder. The relevant equations for the situation in which \mathbf{M} is perpendicular to the symmetry axis are summarized in the appendix. On the other hand, if $m^* = 0$ then ϕ_m (and hence \mathbf{H} , \mathbf{F}_{un} , and \mathbf{F}_{sat}) will tend to zero more rapidly. Examples of both types of behaviour are presented in the discussion that follows.

3. Planar periodically magnetized structures

Consider an infinite slab of hard ferromagnetic material with thickness $2b$ magnetized such that $\mathbf{M} = M_y(x) \hat{j}$, where \hat{j} is a unit vector normal to the surface and

$$M_y(x) = M_0 \cos(kx) \quad (8)$$

as illustrated in figure 1. The magnetic scalar potential associated with this distribution of magnetization is

$$\phi_m(x, y) = \frac{M_0}{k} \cos(kx) \sinh(kb) \exp(-ky) \quad (9)$$

for $y \geq b$ [18]. The corresponding magnetic field $\mathbf{H} = H_x \hat{i} + H_y \hat{j}$ has components

$$H_x = k \tan(kx) \phi_m(x, y) \quad H_y = k \phi_m(x, y) \quad (10)$$

and spatial derivatives

$$\begin{aligned} \frac{\partial H_x}{\partial x} &= k^2 \phi_m(x, y) & \frac{\partial H_y}{\partial y} &= -k^2 \phi_m(x, y) \\ \frac{\partial H_x}{\partial y} &= \frac{\partial H_y}{\partial x} & &= -k^2 \tan(kx) \phi_m(x, y). \end{aligned} \quad (11)$$

The magnetostatic forces exerted on point-like magnetic particles located in the vicinity of the slab are thus

$$\mathbf{F}_{\text{un}} = -\mu_0 \beta M_0^2 k \sinh^2(kb) \exp(-2ky) \hat{j} \quad (12)$$

and

$$\mathbf{F}_{\text{sat}} = -\mu_0 m_s M_0 k \sinh(kb) \exp(-ky) \hat{j} \quad (13)$$

for the unsaturated (cf equation (3)) and saturated (cf equation (5)) limits, respectively.

Several observations relevant to equations (12) and (13) are worth noting. First, the geometry pictured in figure 1 results in magnetostatic forces that are (a) independent of the transverse coordinate x and (b) solely directed normal to the magnetized slab (i.e. $F_x = F_z = 0$). Second, it is clear that a thick slab always exerts a larger force than a thin

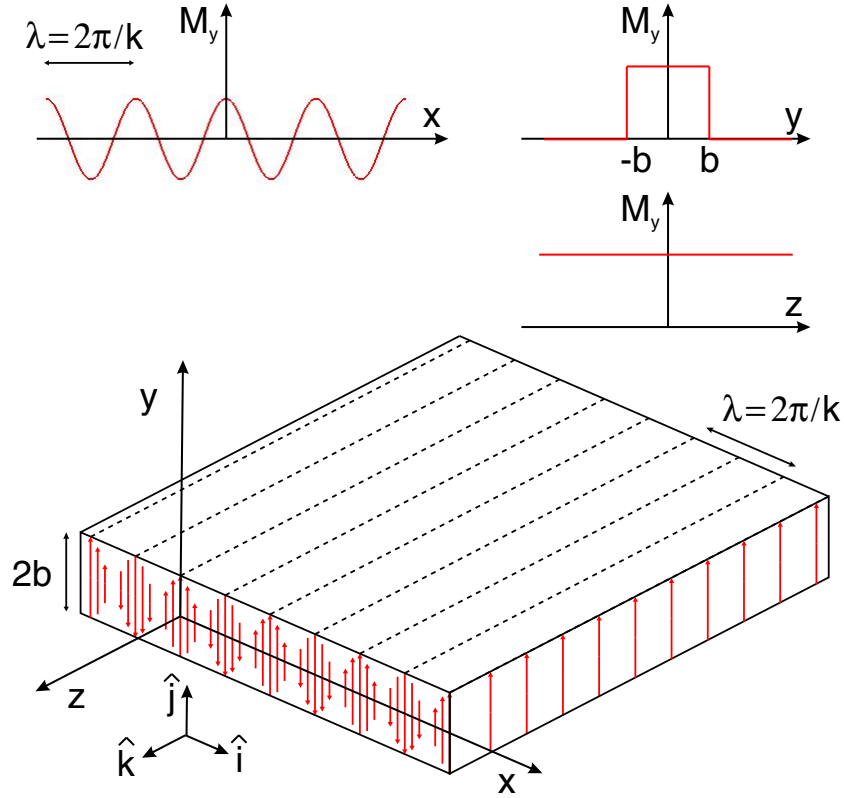


Figure 1. An infinite slab of hard ferromagnetic material magnetized such that \mathbf{M} is normal to the surface and varies as $\cos(2\pi x/\lambda)$ along one of the transverse spatial coordinates. The force exerted on a small magnetic body placed anywhere above (or below) this slab only depends on the y coordinate and is always directed normal the slab.

slab; this point is discussed further in the following section. Third, the magnetostatic force decreases exponentially as a function of the coordinate y . The characteristic length scale for this attenuation is governed by the spatial periodicity of \mathbf{M} , with long wavelength variations (small $k = 2\pi/\lambda$) resulting in better penetration into the surrounding media at the expense of reduced maximum forces. For a given slab thickness $2b$ the maximum force at elevation $y > b$ is obtained for the value of k that satisfies

$$\frac{\alpha}{2} - ky + \frac{kb}{\tanh kb} = 0, \quad (14)$$

where $\alpha = 1$ for unsaturated magnetic particles and $\alpha = 2$ for saturated magnetic particles. In the limit $kb \ll 1$, these maxima exist for real values of k satisfying

$$k'_{\text{un}} = \frac{3}{2b} \left(\frac{y}{b} - \sqrt{\frac{y^2}{b^2} - 2} \right) \quad \text{and} \quad k'_{\text{sat}} = \frac{3}{2b} \left(\frac{y}{b} - \sqrt{\frac{y^2}{b^2} - \frac{24}{9}} \right) \quad (15)$$

which reduce to

$$k'_{\text{un}} = \frac{3}{2y} \quad \text{and} \quad k'_{\text{sat}} = \frac{2}{y} \quad (16)$$

for large values of y/b . Finally we note that, for a given geometry, the characteristic length scale over which magnetostatic forces exerted on permanently magnetized (saturated) particles are attenuated is double that for unsaturated particles.

4. Flux enhancement

The magnitude of the force that can be exerted by the magnetization distribution pictured in figure 1 increases in proportion to $\sinh(kb)$ or $\sinh^2(kb)$, depending on whether the dipole moment of the particle in question is permanent or induced. As the thickness of the magnetized slab increases, so does the magnetic flux emanating from any point along either the top or bottom surface. One way of improving the trapping efficiency of this ‘magnetic bandage’ is to force all of the flux to emanate from only one of the two surfaces [11, 13]. This can be accomplished by imposing an in-plane magnetization component that is in spatial quadrature with the transverse component. That is, if the magnetization of the slab described in the previous section becomes

$$\mathbf{M} = -M_0 \sin(kx) \hat{i} + M_0 \cos(kx) \hat{j} \quad (17)$$

as illustrated in figure 2, the magnetic flux above the slab is doubled and that below the slab becomes identically zero. Changing the sign of the in-plane (i.e. \hat{i}) component of \mathbf{M} causes the flux to emanate from the lower surface. This is nothing other than the principle underlying the design of rubberized ‘refrigerator’ magnets. As far as our analysis is concerned, the magnetic scalar potential corresponding to equation (17) is simply double that given by equation (9) [18]. This in turn implies that the magnetostatic forces are four times as large as that given by equation (12) in the unsaturated case and double that given by equation (13) in the saturated case. That is

$$\mathbf{F}_{\text{un}} = -4\mu_0\beta M_0^2 k \sinh^2(kb) \exp(-2ky) \hat{j} \quad (18)$$

and

$$\mathbf{F}_{\text{sat}} = -2\mu_0 m_s M_0 k \sinh(kb) \exp(-ky) \hat{j} \quad (19)$$

for the magnetized slab pictured in figure 2.

Clearly the development of magnetic bandages with continuously varying magnetization vectors is not a trivial task. On the other hand, an appropriate arrangement of discrete magnets aligned so as to mimic the magnetization distribution required by equation (17) is a relatively simple task. Such arrays are often referred to as Halbach arrays [12], and they have been used in applications ranging from undulators for particle accelerators to magnetic levitation devices. A few examples are pictured in figure 3.

5. Figure of merit and comparison of magnetized structures

The relative trapping efficiency of various magnetized structures can be compared by introducing appropriate figures of merit. A convenient dimensionless quantity relevant to trapping particles in the unsaturated (linear induced dipole moment) limit is

$$\frac{F_{\text{un}} L}{\mu_0 \beta M_0^2} \equiv \frac{L \nabla |\nabla \phi_m|^2}{M_0^2}, \quad (20)$$

where L is a characteristic dimension of the magnet. An analogous parameter for particles in the saturated (permanent dipole moment) limit is

$$\frac{F_{\text{sat}} L}{\mu_0 m_s M_0} \equiv \frac{L \nabla |\nabla \phi_m|}{M_0}. \quad (21)$$

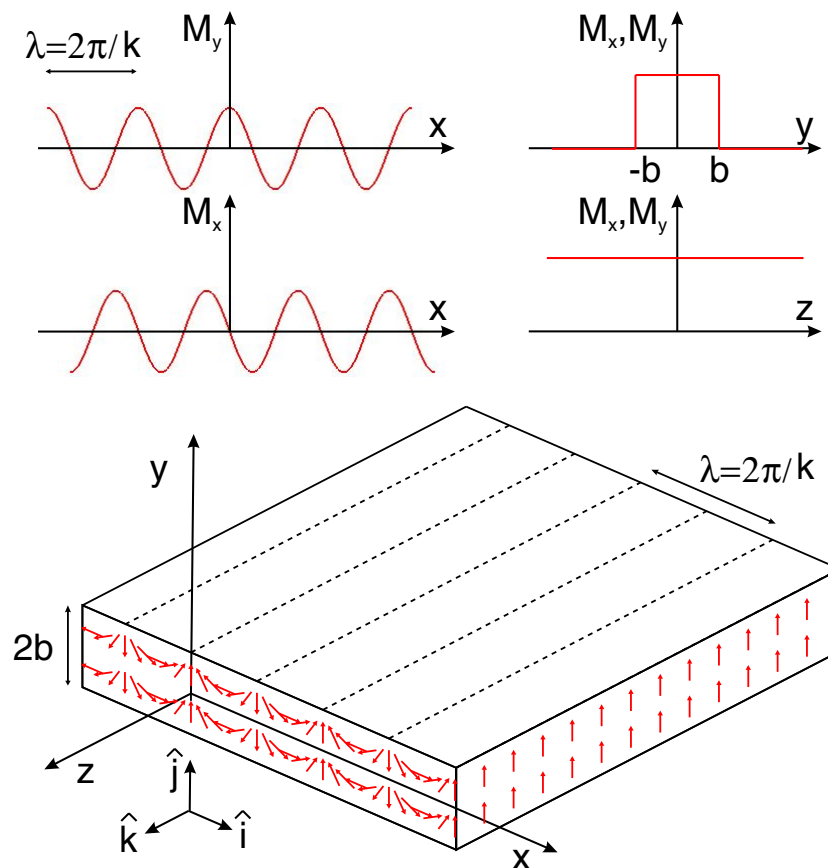


Figure 2. The magnetic scalar potential above the infinite magnetized slab shown in figure 1 is doubled when an in-plane magnetization component is superimposed in quadrature to the normal component (cf equation (17)). At the same time, the magnetic flux emanating from the lower surface is eliminated. Note that the magnitude of the magnetization vector is uniform throughout the slab in this configuration; only its direction changes.

Both of these quantities parameterize the contribution of geometric factors (i.e. the distribution of magnetization within the source—or relative to the ROI) to the force that can be exerted on point-like magnetic particles.

Figure 4 summarizes the geometry of six magnetized structures, each of which is assumed to be infinitely long in the third dimension. Four of these structures are uniformly magnetized throughout their volume, and are intended as being representative of ‘conventional’ magnets. The other two have been designed as one-sided flux structures. Our selection of conventional magnet geometries is motivated by the fact that analytic expressions for the forces that would be exerted on highly magnetic point-like particles located in their vicinity (analogous to equations (18) and (19)) are readily derived, as summarized in the appendix. It is also motivated by the expectation that long uniformly magnetized rods with elliptical cross sections are reasonable facsimiles of long bar magnets.

Figure 5 illustrates the manner in which the figures of merit defined by equations (20) and (21) vary as a function of distance y from the surface of each magnet pictured in figure 4. It is obvious that—for a given magnetization density—the two one-sided flux structures ((b)

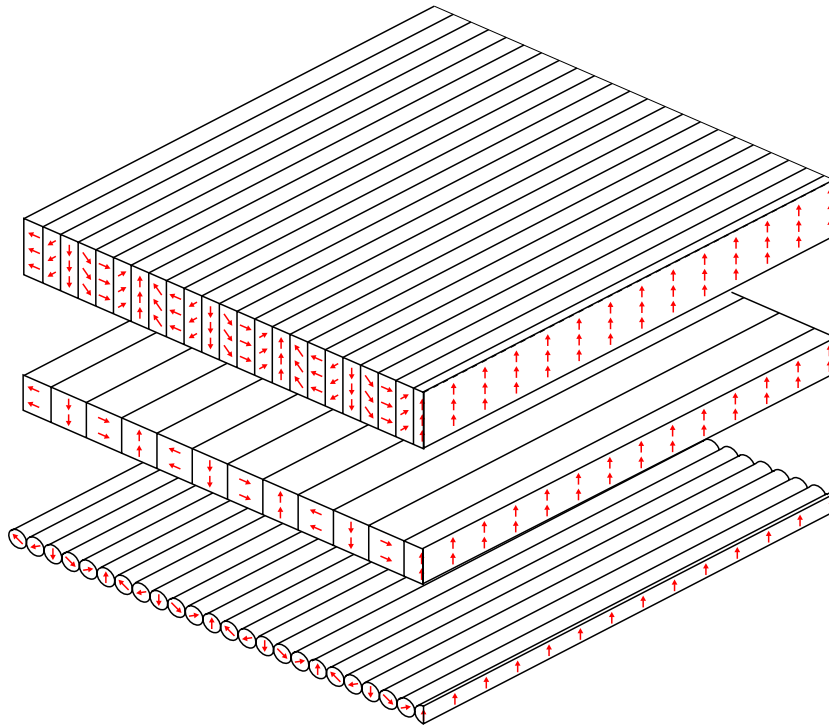


Figure 3. Examples of discrete magnetization arrays that approximate the continuous distribution shown in figure 2. In each case the flux is enhanced above the array and reduced below the array. The topmost example requires the use of bar magnets magnetized at odd angles. The middle example is a conventional Halbach configuration. Some degree of flux cancellation is sacrificed for ease of construction. The bottom example enables one to achieve better control over the direction and periodicity of the magnetization vector, and it can be constructed from a single type of magnet. Unlike the ideal one-sided flux array, all of these structures subject point-like magnetic particles to forces that do depend somewhat on the transverse spatial coordinate.

and (d)) outperform the conventional structures at short range, and that the opposite is true at large distances. Several factors contribute to this difference. At short range, the forces exerted by the one-sided flux structures are larger both because the magnetic flux is forced to loop back to the magnet surface on a length scale determined by the periodicity of the magnetization vector *and* because all of the flux is forced to emanate from a single surface. On the other hand the magnitude of these forces decreases exponentially as a function of distance, consistent with the fact that neither structure has a net magnetic moment. The figures of merit for the other four structures decrease more slowly, converging to a $\propto 1/y^5$ behaviour at large distances, consistent with the fact that each one does possess a net magnetic moment. Note that the cross sectional areas (and hence the net magnetic moments) of the magnets shown in panels (a), (c) and (e) of figure 4 are identical.

Comparisons between the figures of merit for various combinations of structures are instructive. For example, the characteristic transverse dimension over which magnetic flux emanates from the structures in panels (a) and (b) is the same (i.e. $2L$). On the other hand, the return paths for this flux are completely different. All of the magnetic flux emanating from the one-sided flux structure is forced to loop back to the magnet surface over a transverse distance of no more than $2L$, while no such constraint exists for the cylinder. The result is

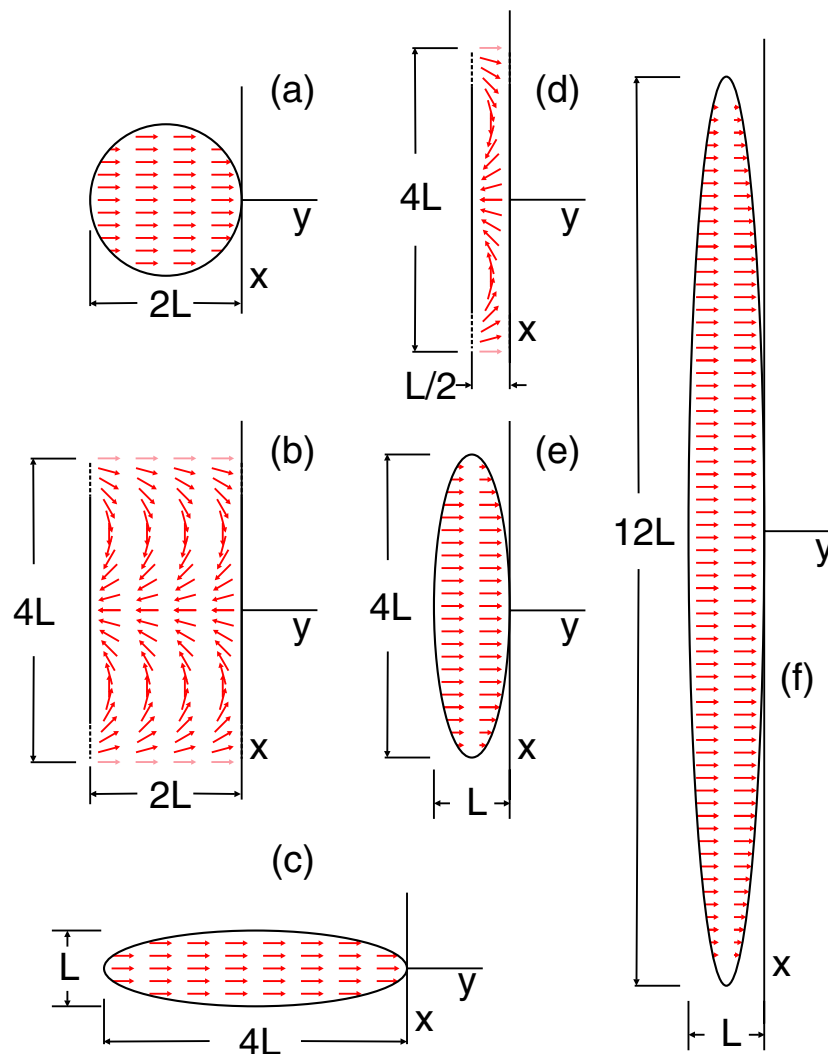


Figure 4. Cross sections for the six magnetic structures that are compared for their relative trapping efficiencies in figure 5. In each case the magnetization density is uniform, and the origin of the coordinate system is located at the surface of the magnet. Panel (a) shows an infinitely long cylinder of radius L uniformly magnetized perpendicular to its axis. Panel (b) shows an infinite two-dimensional slab of material in which the direction of the magnetization vector rotates so that all of the flux emanates from the right-hand surface. Both the thickness of the slab and the length scale over which the magnetization vector changes direction ($\lambda/2$) have been set equal to the diameter of the cylinder shown in panel (a). Panel (c) shows an infinitely long rod with an elliptical cross section uniformly magnetized perpendicular to its axis. The area (and hence the magnetic moment) of this structure is the same as that of the cylindrical magnet. Panel (d) shows an infinite magnetized slab identical to that shown in panel (b), except that its thickness has been reduced by a factor of four. Panel (e) shows another infinitely long elliptical rod, in which the major and minor axes have been interchanged with respect to panel (c). Panel (f) shows a similar elliptical magnet, except that the major axis has been elongated considerably.

an enhancement in both \mathbf{F}_{un} and \mathbf{F}_{sat} at short range. Clearly another factor that contributes to the dramatic difference in the figures of merit for structures (a) and (b) is the simple fact that

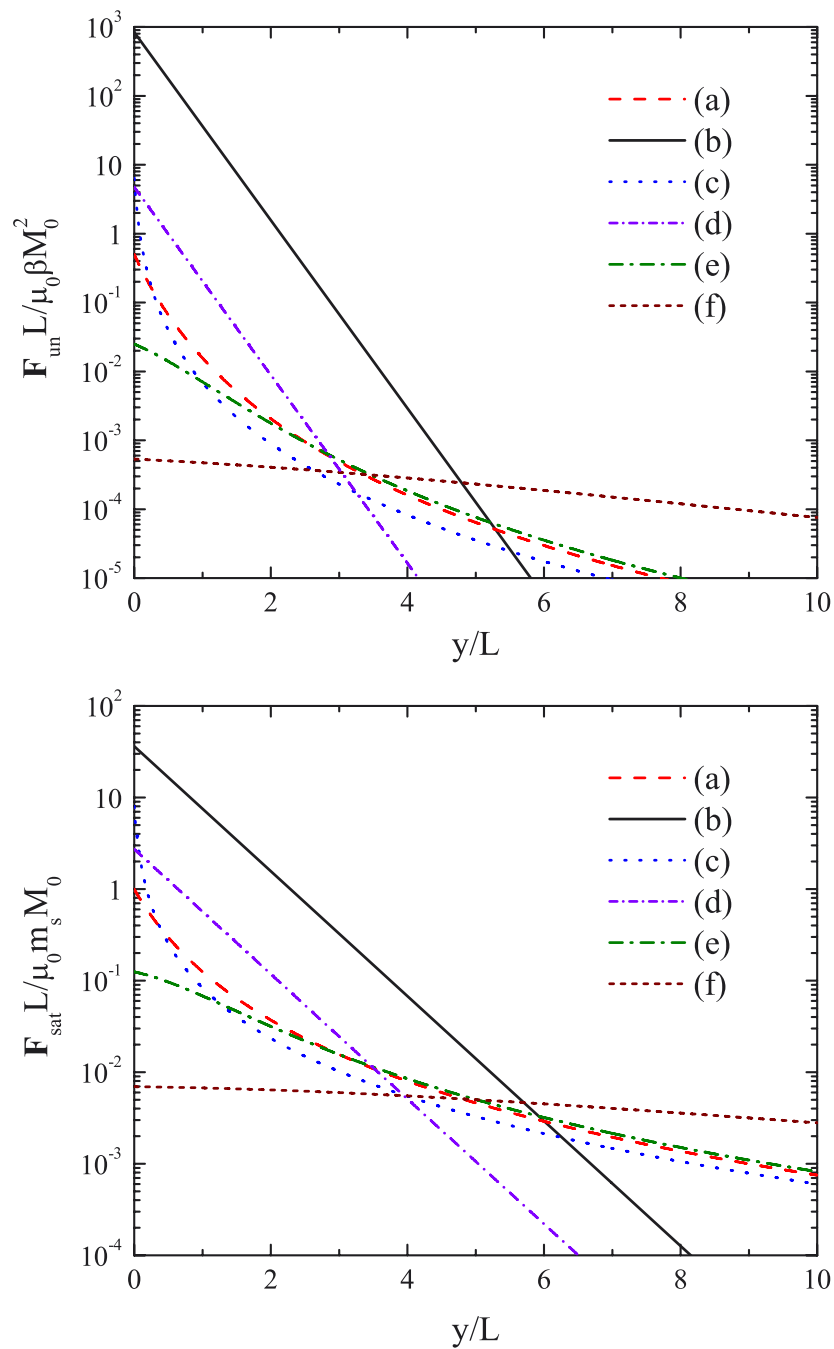


Figure 5. Dimensionless figures of merit for the various magnetized structures shown in figure 4. The top panel summarizes results for unsaturated magnetic particles while the bottom panel shows equivalent results for saturated magnetic particles. There is a one-to-one correspondence between the labels (a)–(f) that appear in this figure and those used in figure 4.

structure (b) is physically much larger. Regardless, the thinner one-sided flux structure shown in panel (d) still outperforms the four conventional magnets at short range, and would continue

to do so even if truncated so as to have the same cross sectional area as the cylinder. The elliptical structures shown in panels (c) and (e) can either be viewed as deformed versions of the cylinder, or as approximations for rectangular bar magnets. From the former viewpoint, comparison of the figures of merit for the structures shown in panels (a), (c), and (e) reveals the short-range nature of changes in \mathbf{F}_{un} and \mathbf{F}_{sat} associated with modifications to the distribution of magnetization within the source. Differences between these three cases at large distances are due solely to the fact that the centre-of-mass positions of structures (a), (c), and (e) are not equivalent. From the latter viewpoint, comparison of the results for the structures shown in panels (e) and (f) shows the trend as the transverse dimension (and total magnetization) of a conventional magnet is increased. Ultimately, this does not represent an efficient strategy for exerting large magnetostatic forces; the magnetic field produced by an infinite uniformly magnetized plane is also uniform, resulting in a situation where both figures of merit are identically zero.

6. Conclusion

The characteristics of one-sided flux arrays summarized in the previous sections suggest that they hold considerable promise for use in targeting or controlling the delivery of therapeutic agents attached to small magnetic particles. For a given magnetization density and comparable thicknesses, they tend to exert much greater magnetostatic forces on nearby point-like magnetic particles than those that can be achieved with ‘conventional’ magnetic structures. They are thus attractive from the viewpoint of trapping efficiency. Conversely, a relatively thin one-sided flux array can exert short-range forces comparable to those exerted by a much thicker conventional magnet. This could prove advantageous and/or convenient in some clinical applications, and motivates our use of the generic term ‘magnetic bandage’. The forces exerted by one-sided flux structures are directed toward the magnet at every point in space, and are uniform in magnitude at a given distance from its surface. These characteristics may be beneficial both for the design and the interpretation of well-controlled magnetic trapping experiments. At the same time, the more rapid attenuation of forces exerted by one-sided flux structures relative to those exerted by conventional magnets (a consequence of having zero net magnetic moment) may facilitate efforts to achieve uniform deposition of therapeutic agents through the use of carriers with an appropriate (non-uniform) distribution of magnetic and physical properties. Finally, the mere fact that remarkably simple analytic expressions for the relevant magnetostatic forces exist enhances the utility of one-sided flux structures in models of trapping dynamics that attempt to account for hydrodynamic and physiological factors.

We re-emphasize that the focus of our investigation has largely been to explore the potential utility of one-sided flux structures for magnetic trapping applications at a conceptual level. We have ignored material properties (both as they apply to the manufacture of real one-sided flux structures and as they apply to the behaviour of real magnetic microparticles and/or nanoparticles), choosing instead to examine magnetostatic forces in two somewhat idealized limits (referred to as ‘unsaturated’ and ‘saturated’ material responses). We have likewise restricted our discussion to the limit in which the density of magnetic particles within the bloodstream remains low, ignoring particle–particle interactions and any modification of the fields that results from their introduction.

Acknowledgments

MH is grateful to C P Bidinosti for useful discussions and wishes to thank members of the Département de Physique de l’Ecole Normale Supérieure (Paris) for their hospitality during

the preparation of this manuscript. We acknowledge funding support from the Natural Sciences and Engineering Research Council of Canada and the Canadian Institutes of Health Research.

Appendix. Infinitely long uniformly magnetized rods

We have made use of infinitely long uniformly magnetized rods as examples of ‘conventional’ magnets against which trapping efficiency (characterized by the figure of merit defined in section 5) of one-sided flux structures can be compared. This appendix summarizes relevant equations for the magnetic scalar potential, magnetic field, and magnetostatic forces exerted on point-like magnetic particles in the vicinity of such rods. Complementary information can be found in textbooks on electromagnetism.

A.1. Rod with circular cross section

The magnetic scalar potential in the vicinity of an infinitely long circular cylinder with radius R and uniform transverse magnetization \mathbf{M} is given by [18–20]

$$\phi_m = \frac{M R^2}{2 \rho} \cos \phi \quad \text{for } \rho \geq R, \quad (22)$$

where ρ and ϕ represent the radial and polar coordinates of an arbitrary point with respect to a polar coordinate system coincident with the axis of the cylinder and aligned with respect to \mathbf{M} , as shown in figure A.1. The corresponding magnetic field is given by

$$\mathbf{H} = \frac{M R^2}{2 \rho^2} (\cos \phi \hat{\rho} + \sin \phi \hat{\phi}), \quad (23)$$

where $\hat{\rho}$ and $\hat{\phi}$ are the appropriate unit vectors. This is identical to the field produced by a uniform linear array of dipolar sources with a magnetic moment per unit length $\pi R^2 M$. The magnetostatic force exerted on a point-like magnetic particle in the vicinity of the cylinder is thus

$$\mathbf{F}_{\text{un}} = -\frac{\mu_0 \beta M^2 R^4}{4 \rho^5} \left[(1 + \cos^2 \phi) \hat{\rho} + \frac{1}{2} \sin 2\phi \hat{\phi} \right] \quad (24)$$

in the unsaturated (linear induced dipole moment) limit (cf equation (3)) and

$$\mathbf{F}_{\text{sat}} = -\frac{\mu_0 m_s M R^2}{2 \rho^3} \left[(1 + \cos^2 \phi) \hat{\rho} + \frac{1}{2} \sin 2\phi \hat{\phi} \right] \quad (25)$$

in the saturated (permanent dipole moment) limit (cf equation (5)).

A.2. Rod with ellipsoidal cross section

The magnetic scalar potential in the vicinity of an infinitely long elliptical cylinder with semi-major axis a , semi-minor axis b , and uniform transverse magnetization \mathbf{M} can be written as [20]

$$\phi_m = \frac{Mab}{\sqrt{a^2 - b^2}} \exp(-\xi) \cos(\eta - \beta) \quad \text{for } \xi \geq \xi_0, \quad (26)$$

where ξ and η represent the radial and polar analogues of ρ and ϕ in an elliptical coordinate system [21] coincident with the axis of the cylinder as shown in figure A.2, and β represents the polar angle between \mathbf{M} and the semi-major axis of the ellipse. Curves along which ξ or η are constant are families of confocal ellipses and hyperbolae, respectively. The curve $\xi_0 = \tanh^{-1}(a/b)$ is coincident with the surface of the magnetized ellipse while $\eta = 0, \pi/2$,

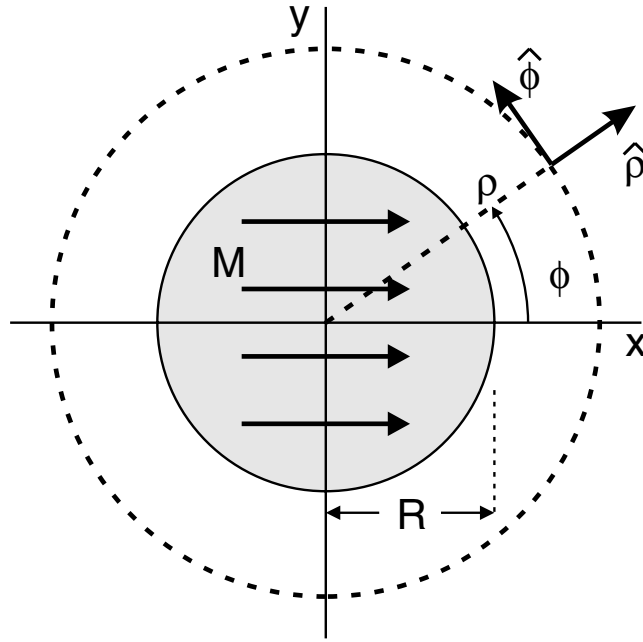


Figure A.1. Cross section through an infinitely long cylinder of radius R uniformly magnetized perpendicular to its axis.

π , and $3\pi/2$ correspond to the $+x$, $+y$, $-x$, and $-y$ axes of the Cartesian coordinate system of figure A.2. More generally the correspondence between these coordinate systems is such that

$$x = f \cosh \xi \cos \eta \quad \text{and} \quad y = f \sinh \xi \sin \eta, \quad (27)$$

where $f = \sqrt{a^2 - b^2}$.

The magnetic field corresponding to the scalar potential described by equation (26) is given by

$$\mathbf{H} = \frac{Mab}{a^2 - b^2} \exp(-\xi) \left[\frac{\cos(\eta - \beta) \hat{\xi} + \sin(\eta - \beta) \hat{\eta}}{\sqrt{\sinh^2 \xi + \sin^2 \eta}} \right], \quad (28)$$

where the unit vectors $\hat{\xi}$ and $\hat{\eta}$ are related to the unit vectors $\hat{\rho}$ and $\hat{\phi}$ of a polar coordinate system such that

$$\hat{\xi} = \frac{f}{\rho} \left[\frac{\sinh \xi \cosh \xi \hat{\rho} + \sin \eta \cos \eta \hat{\phi}}{\sqrt{\sinh^2 \xi + \sin^2 \eta}} \right] \quad (29)$$

and

$$\hat{\eta} = \frac{f}{\rho} \left[\frac{-\sin \eta \cos \eta \hat{\rho} + \sinh \xi \cosh \xi \hat{\phi}}{\sqrt{\sinh^2 \xi + \sin^2 \eta}} \right]. \quad (30)$$

In the limit that the eccentricity $e = f/a = \sqrt{1 - b^2/a^2}$ of the ellipse is reduced to zero, $\exp(-\xi)/f$ remains finite while $\hat{\xi} \rightarrow \hat{\rho}$ and $\hat{\eta} \rightarrow \hat{\phi}$. At the same time equations (26) and (28) reduce to equations (22) and (23), respectively, for $\beta = 0$.

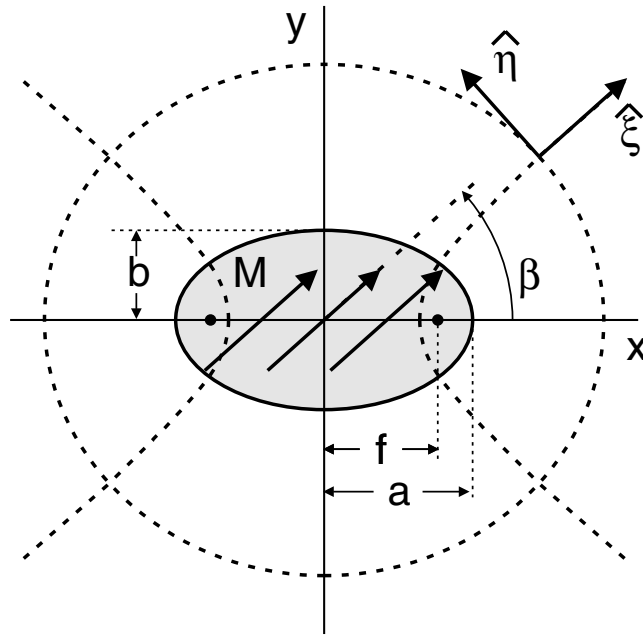


Figure A.2. Cross section through an infinitely long ellipse uniformly magnetized at an angle β with respect to its semi-major axis. The foci of the ellipses and hyperbolae are given by $f = \pm\sqrt{a^2 - b^2}$.

Finally, the force exerted on a point-like magnetic particle is

$$\mathbf{F}_{\text{un}} = -\frac{\mu_0 \beta M^2 a^2 b^2}{(a^2 - b^2)^{5/2}} \frac{\exp(-2\xi)}{[\sinh^2 \xi + \sin^2 \eta]^{3/2}} \times \left\{ \left[1 + \frac{\sinh \xi \cosh \xi \cos^2(\eta - \beta)}{\sinh^2 \xi + \sin^2 \eta} + \frac{\sin 2\eta \sin[2(\eta - \beta)]}{4(\sinh^2 \xi + \sin^2 \eta)} \right] \hat{\xi} + \left[\frac{\sinh \xi \cosh \xi \sin[2(\eta - \beta)]}{2(\sinh^2 \xi + \sin^2 \eta)} + \frac{\sin^2(\eta - \beta) \sin 2\eta}{2(\sinh^2 \xi + \sin^2 \eta)} \right] \hat{\eta} \right\} \quad (31)$$

in the unsaturated limit (cf equation (3)) and

$$\mathbf{F}_{\text{sat}} = -\frac{\mu_0 m_s M a b}{(a^2 - b^2)^{3/2}} \frac{\exp(-\xi)}{[\sinh^2 \xi + \sin^2 \eta]} \times \left\{ \left[1 + \frac{\sinh \xi \cosh \xi \cos^2(\eta - \beta)}{\sinh^2 \xi + \sin^2 \eta} + \frac{\sin 2\eta \sin[2(\eta - \beta)]}{4(\sinh^2 \xi + \sin^2 \eta)} \right] \hat{\xi} + \left[\frac{\sinh \xi \cosh \xi \sin[2(\eta - \beta)]}{2(\sinh^2 \xi + \sin^2 \eta)} + \frac{\sin^2(\eta - \beta) \sin 2\eta}{2(\sinh^2 \xi + \sin^2 \eta)} \right] \hat{\eta} \right\} \quad (32)$$

in the saturated limit (cf equation (5)). Note that the last term in each set of square brackets within equations (31) and (32) is attenuated exponentially as a function of distance; all four of these terms vanish as the eccentricity of the ellipse is reduced to zero. The remaining terms reduce to equations (24) and (25) in this limit if $\beta = 0$, as they should.

References

- [1] Häfeli U O 2004 *Int. J. Pharm.* **277** 19–24
- [2] Lawaczek R *et al* 1997 *Acta Radiol.* **38** 584–97
- [3] Goodwin S, Peterson C, Hoh C and Bittner C 1999 *J. Magn. Magn. Mater.* **194** 132–9
- [4] Alexiou C, Arnold W, Klein R J, Parak F G, Hulin P, Bergemann C, Erhardt W, Waenpfeil S and Lübke A S 2000 *Cancer Res.* **60** 6641–8
- [5] Lübke A S, Alexiou C and Bergemann C 2001 *J. Surg. Res.* **95** 200–6
- [6] Driscoll C F *et al* 1984 *Microvasc. Res.* **27** 353–69
- [7] Grief A D and Richardson G 2005 *J. Magn. Magn. Mater.* **293** 455–63
- [8] Aviles M O, Ebner A D, Chen H T, Rosengart A J, Kaminski M D and Ritter A J 2005 *J. Magn. Magn. Mater.* **293** 605–15
- [9] Rotariu O and Strachan N J C 2005 *J. Magn. Magn. Mater.* **293** 639–46
- [10] Pankhurst Q A, Connolly J, Jones S K and Dobson J 2003 *J. Phys. D: Appl. Phys.* **36** R167–81
- [11] Mallinson J C 1973 *IEEE Trans. Magn.* **9** 678–82
- [12] Halbach K 1980 *Nucl. Instrum. Methods* **169** 1–10
- [13] Shute H A, Mallinson J C, Wilton D T and Mapps D J 2000 *IEEE Trans. Magn.* **36** 440–51
- [14] Halbach K 1985 *J. Appl. Phys.* **57** 3605–8
- [15] Han Q, Ham C and Phillips R 2005 *IEE Proc. Electr. Power Appl.* **152** 535–42
- [16] Earnshaw E 1842 *Trans. Camb. Phil. Soc.* **7** 97–112
- [17] Jackson J D 1975 *Classical Electrodynamics* 2nd edn (Toronto: Wiley)
- [18] Durand E 1968 *Magnétostatique* (Paris: Masson et C^{ie})
- [19] Stratton J A 1941 *Electromagnetic Theory* 1st edn (New York: McGraw-Hill)
- [20] Ferraro V C A 1954 *Electromagnetic Theory* (London: Athlone)
- [21] Abramowitz M and Stegun I A 1970 *Handbook of Mathematical Functions* 9th edn (New York: Dover)